A State Space Formulation for Moving Loads Identification

X. Q. Zhu
Associate Professor
Faculty of Civil Engineering and Architecture,
Zhejiang University of Technology,
Hangzhou, Zhejiang, PRC

S. S. Law
Associate Professor
Hong Kong Polytechnic University,
Hunghom, Hong Kong, PRC

J. Q. Bu
Associate Professor
Shijiazhuang Railway Institution,
Shijiazhuang, Hebei, PRC

A new moving load identification method formulated in state space with regularization on the solution is presented. The bridge deck is modeled as an orthotropic rectangular plate, and the loads are modeled as a group of loads moving on top of the bridge deck at a fixed distance and at a constant speed. The Hamilton principle and the modal superposition principle are included in the formulation. Numerical simulations and experimental tests are employed for the verification and illustration on the effectiveness of the proposed method. The effects of different sensor location, different load path eccentricity, different types of measured information, and measurement noise have been investigated, and the effect of the aspect ratio of the bridge deck is also studied. It is concluded that nine sensors collecting information from nine vibration modes would give reasonably accurate identified results over the practical range of aspect ratio of a modern bridge deck. Acceleration responses are preferred over the velocity and strain responses in this study, and the same type of response should be collected for the same supporting beam in the longitudinal direction. [DOI: 10.1115/1.2202149]

Keywords: moving load, orthotropic plate, bridge deck, state space, dynamics, force identification, inverse problem, ill-conditioned, regularization

1 Introduction

It is important to obtain the information of vehicular load on a highway not only for the bridge design but also for the management of highway pavement. However, calculation or direct measurement of the interaction force between the vehicle and the bridge/road is usually subject to bias. Methods of weigh-in motion using static strain measurement [1] and moving loads identification using dynamic response measurement [2–8] have been developed to meet this need.

A technique on moving load identification from bridge responses has been developed very rapidly in the last few years. The identification problem can be solved in either the time domain [2,7] or the frequency domain [3]. The theoretical basis of the techniques can also be categorized into two kinds, i.e., the exact solution method (ESM) [8] and the finite element method (FEM) [7]. The bridge is generally modeled as a Bernoulli-Euler beam or Timoshenko beam [2,4] or an orthotropic rectangular plate [5,7,8]. The beam model may be a simply supported beam [2,3] or a continuous beam [4]. In practice, the orthotropic rectangular plate model would best represent the real bridge deck. The vehicle is modeled as a suspended system of mass with damping and rigidity or in terms of two axle loads moving at a fixed spacing. The optimal regularization technique [9,15] has been widely used to provide bounds to the ill-conditioned inverse problem in the load identification.

The measured bending moment, strain, displacement, velocity, acceleration of the bridge, or their combination is employed to identify the moving load [2–8,10]. Each type of measured response when used in the identification has its own advantage and disadvantage, and they may be used according to the practical conditions and environments.

The moving load identification problem is formulated in the state space in this paper. This approach is better than other approaches developed by the authors [2–4,7] due to its computational efficiency and the ease of using combination measurements in the identification, in which the measured strain, velocity, and acceleration responses can be used separately or in a combination as input to the identification algorithm. The bridge deck is modeled as an orthotropic rectangular plate, and loads from vehicle are modeled as a group of loads moving on top of the bridge deck at a fixed spacing and at a constant speed. The Hamilton principle and the mode superposition principle are included in the formulation. Computation simulations and laboratory tests are used to illustrate the effectiveness and the validity of the proposed method. The effects of different sensor location, different load path eccentricity, different types of measured information, measurement noise, and the aspect ratio of the bridge deck have been investigated. It is concluded that nine sensors collecting information from nine vibration modes would give reasonably accurate identified results over the practical range of aspect ratio of a modern bridge deck. Acceleration responses are preferred over the velocity and strain responses in the present study, and the same type of response should be collected for the same supporting beam in the longitudinal direction.

Contributed by the Technical Committee on Vibration and Sound of ASME for publication in the JOURNAL OF VIBRATION AND ACOUSTICS. Manuscript received October 9, 2003; final manuscript received February 3, 2006. Assoc. Editor: Chin An Tan.

2 Equation of Motion

2.1 Continuous Time State-Space Equation. The bridge deck is modeled as an orthotropic plate simply supported along $x=0$ and $x=a$ with the other two edges free, and the loads are moving in a group at a constant speed as shown in Fig. 1. The strain energy of the orthotropic plate is

$$U=\frac{1}{2}\int\int_s\left[D_x\left(\frac{\partial^2 w}{\partial x^2}\right)^2+(D_x v_{xy}+D_y v_{yx})\frac{\partial^2 w}{\partial x^2}\frac{\partial^2 w}{\partial y^2}+D_y\left(\frac{\partial^2 w}{\partial y^2}\right)^2+4D_k\left(\frac{\partial^2 w}{\partial x\partial y}\right)^2\right]ds \tag{1}$$

where v_{xy} is the Poisson ratio associated with a strain in the y direction for a load in the x direction, and v_{yx} is similarly defined. D_x and D_y are the flexural rigidities of the orthotropic plate in the x and y directions, respectively. D_k is the torsional rigidity of the orthotropic plate.

The kinetic energy is expressed as

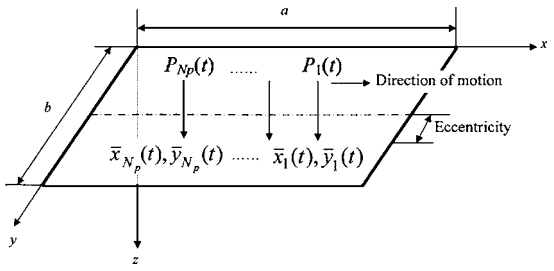

Fig. 1 Orthotropic plate under a group of moving loads

$$T = \frac{1}{2}\int_0^a \int_0^b \dot{w}(x,y,t)^2 \rho h dx dy \tag{2}$$

where $w(x,y,t)$ equals $[\partial w(x,y,t)]/\partial t$. h is the equivalent thickness and ρ is the density of the plate. a and b are the length and width of the plate.

The external work can be written as

$$W = \int_0^a \int_0^b \sum_{l=1}^{N_P} p_l(t)\delta[x - \bar{x}_l(t)]\delta[y - \bar{y}_l(t)]w(x,y,t)dxdy \tag{3}$$

where $\{p_l(t),\ l=1,2,\ldots,N_p\}$ are the moving loads on the bridge deck. $\bar{x}_l(t)$ and $\bar{y}_l(t)$ define the position of moving load $p_l(t)$ at time t. $\delta(x)$ and $\delta(y)$ are the Dirac functions.

The work done due to damping in the plate is given by

$$W_c = -\int_0^a \int_0^b w(x,y,t)c_b \dot{w}(x,y,t)dxdy \tag{4}$$

where c_b is the damping coefficient of the plate.

The displacement is then represented by a series of products of beam function based on the modal superposition principle

$$w(x,y,t) = \sum_{i,j} \phi_{ij}(x,y)q_{ij}(t) = \sum_{i,j} \psi_i(x)\varphi_j(y)q_{ij}(t) \tag{5}$$

where $\psi_i(x)$, $\varphi_j(y)$ $(i=1,2,\ldots,m;\ j=1,2,\ldots,n)$ are the normal modes of the plate with appropriate boundary conditions. $q_{ij}(t)$ is the corresponding amplitude.

Equation (5) can be written in matrix form as

$$w(x,y,t) = \phi Q \tag{6}$$

where

$$\phi = \{\psi_1(x)\varphi_1(y), \psi_1(x)\varphi_2(y), \ldots, \psi_1(x)\varphi_n(y), \psi_2(x)\varphi_1(y), \ldots, \psi_m(x)\varphi_n(y)\}$$

$$Q = \{q_{11}(t), q_{12}(t), \ldots, q_{1n}(t), q_{21}(t), \ldots, q_{mn}(t)\}^T$$

The strains in x direction in the plate at point (x,y) and time t are obtained from Eq. (5) as

$$\varepsilon_x(x,y,t) = \theta Q$$

$$\theta = \{z_t\ddot{\psi}_1(x)\varphi_1(y), z_t\ddot{\psi}_1(x)\varphi_2(y), \ldots, z_t\ddot{\psi}_1(x)\varphi_n(y), z_t\ddot{\psi}_2(x)\varphi_1(y), \ldots, z_t\ddot{\psi}_m(x)\varphi_n(y)\} \tag{7}$$

where z_t is the distance from the neutral axis to the bottom tension surface, and $\ddot{\psi}_i(x)$ is the second derivative of $\psi_i(x)$ with respect to x. The strains in the y direction can be similarly defined.

Substitute Eq. (5) into Eqs. (1)–(4), and with the Hamilton principle

$$\delta\int_{t_1}^{t_2}(T-U)dt + \delta\int_{t_1}^{t_2}(W+W_e)dt = 0$$

The equation of motion can be obtained as

$$M\ddot{Q} + C\dot{Q} + KQ = P \tag{8}$$

where $M_{(mn)(mn)}$, $C_{(mn)(mn)}$, and $K_{(mn)(mn)}$ are the mass, damping and stiffness matrices. P is a $(mn\times 1)$ normalized force vector. Q, $\dot{Q}$, and $\ddot{Q}$ are $(mn\times 1)$ vectors.

$$M = \int_0^a \int_0^b \rho h \phi^T \phi dxdy$$

$$C = \int_0^a \int_0^b \phi^T c_b \phi dxdy$$

$$K = \int_0^a \int_0^b \left\{ D_x \left[\frac{\partial^2\phi}{\partial x^2}\right]^T \left[\frac{\partial^2\phi}{\partial x^2}\right] + [D_x v_{xy} + D_y v_{yx}] \left[\frac{\partial^2\phi}{\partial x^2}\right]^T \left[\frac{\partial^2\phi}{\partial y^2}\right] + D_y \left[\frac{\partial^2\phi}{\partial y^2}\right]^T \left[\frac{\partial^2\phi}{\partial y^2}\right] + 4D_k \left[\frac{\partial^2\phi}{\partial x\partial y}\right]^T \left[\frac{\partial^2\phi}{\partial x\partial y}\right] \right\} dxdy \tag{9}$$

P is rewritten as

$$P = \phi_p p \tag{10}$$

where

$$\phi_p = \lfloor \phi(\bar{x}_1(t),\bar{y}_1(t))^T\ \phi(\bar{x}_2(t),\bar{y}_2(t))^T\ \cdots\ \phi(\bar{x}_{N_p}(t),\bar{y}_{N_p}(t))^T \rfloor_{(mn\times N_p)}$$

and

$$p = \{p_1(t)\ p_2(t)\ \cdots\ p_{N_p}(t)\}^T$$

Equation (8) can be written in state space form as

$$\dot{Z} = \bar{K}Z + B_c\phi_p p \tag{11}$$

where

$$Z = \begin{bmatrix} Q \\ \dot{Q} \end{bmatrix}_{(2mn\times 1)};\quad \bar{K} = \begin{bmatrix} 0 & I \\ -M^{-1}K & -M^{-1}C \end{bmatrix}_{(2mn\times 2mn)};\quad B_c = \begin{bmatrix} 0 \\ M^{-1} \end{bmatrix}_{(2mn\times mn)} \tag{12}$$

The state matrix in Eq. (11) is nonsymmetric, but it does not pose any numerical difficulty in the solution. If the response of the orthotropic plate is represented by N_s output quantities in the output vector $v(t)$ from sensors such as accelerometers, velocity transducers, displacement transducers, strain gages, etc., an output equation can be expressed as

$$v = R_a\ddot{Q} + R_v\dot{Q} + R_d Q \tag{13}$$

where R_a, R_v, and R_d are output influence matrices for acceleration, velocity, and strain/displacement, measurements, respectively. Solving for $\ddot{Q}$ from Eq. (8) and substituting into Eq. (13) to yield

$$v = RZ + D\phi_p p \tag{14}$$

where

$$R = [R_d - R_a M^{-1}K\ R_v - R_a M^{-1}C];\quad D = R_a M^{-1} \tag{15}$$

2.2 Discrete Time State Space Model. Equations (11) and (14) are converted into discrete equations using the exponential matrix, and the final discrete model is

$$Z(j+1) = AZ(j) + B\phi_p(j)p(j)$$

$$v(j) = RZ(j) + D\phi_p(j)p(j) \quad (j = 1,2, \ldots ,N) \tag{16}$$

where N is the total number of sampling points, τ is the time step between the variable states $Z(j+1)$ and $Z(j)$, and

$$A = \exp(\bar{K}\tau); \quad B = \bar{K}(A - I)B_c$$

Solving for the output with zero initial conditions from Eq. (16) in terms of the previous inputs $\phi_p(j)$ and $p(i)$ $(i=1,2,\ldots,j)$ yields

$$v(j) = \sum_{i=0}^{j} H_i \phi_p(j-i)p(j-i) \tag{17}$$

where

$$H_0 = D; \quad H_i = RA^{(i-1)}B \tag{18}$$

The constant matrices in the series are known as system Markov parameters. The Markov parameters are commonly used as the basis for identifying mathematical models in linear dynamic systems. The Markov parameters represent the response of the discrete system to unit impulse, and they must be unique for the system [9].

3 Moving Load Identification

Rewrite Eq. (17) to give the matrix convolution equation as

$$\bar{H}P = V \tag{19}$$

where

$$\bar{H} = \begin{bmatrix} H_0\phi_p(0) & 0 & \cdots & 0 \\ H_1\phi_p(0) & H_0\phi_p(1) & \cdots & 0 \\ \vdots & \vdots & \cdots & 0 \\ H_{N-1}\phi_p(0) & H_{N-2}\phi_p(1) & \cdots & H_0\phi_p(N-1) \end{bmatrix}$$

$$P = \{p(0)^T, p(1)^T, \ldots, p(N-1)^T\}^T$$

$$V = \{v(0)^T, v(1)^T, \ldots, v(N-1)^T\}^T$$

This is an ill-posed problem due to the lack of continuous dependence of the solution on the data when the loads are on the supports. A straightforward least-squares solution produces an unbounded result at these locations. Regularization is usually used to circumvent the problem of the lack of continuous dependence. A regularization technique would provide an analysis on the ill-posed problem. One approach to regularization proposed by Tikhonov [15] is to replace Eq. (19) with the associated equation

$$[\bar{H}^T\bar{H} + \lambda I]P = \bar{H}^T V \tag{20}$$

For $\lambda > 0$, the matrix operator $[\bar{H}^T\bar{H} + \lambda I]$ is unique, and therefore, its inverse is continuous. Solving Eq. (20) is equivalent to solving the following unique problem:

$$\min J(P,\lambda) = \|\bar{H}P - V\|^2 + \lambda\|P\|^2 \tag{21}$$

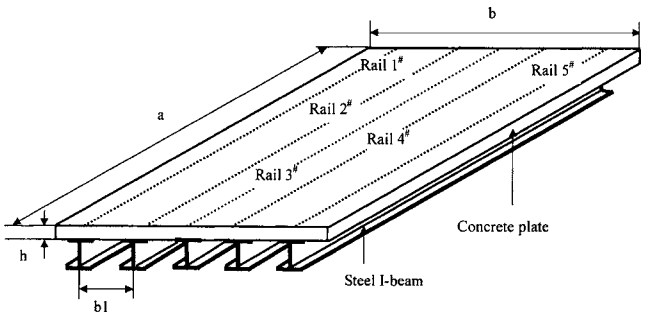

Fig. 2 A typical single-span bridge deck

It is clear from the second term that the non-negative regularization parameter has the effect of forcing a bounded solution. If the measured displacements, velocities, strains, and accelerations (or their combinations) are used together to identify the moving loads, each response component in the vector $v(t)$ in Eq. (13) should be scaled by their respective norms to have dimensionless units.

4 Numerical Simulation

An orthotropic bridge deck simply supported along $x=0$ and $x=a$, with the other two edges free, is studied. The structure consists of five I-section steel beams and a concrete slab as shown in Fig. 2. The natural frequencies and physical parameters of the structure are listed in Tables 1 and 2, respectively. There are five guide rails on the bridge deck for vehicle movement. Rails 1, 2, 3, 4, and 5 correspond to $1/8b$, $3/8b$, $1/2b$, $5/8b$, and $7/8b$, respectively, measured from the left edge of the deck. The rigidities of the equivalent orthotropic plate can be calculated [7] as $D_x = 2.415 \times 10^9$ Nm, $D_y = 2.1813 \times 10^7$ Nm, and $D_k = 2.2195 \times 10^8$ Nm. Sensors are located at the bottom of the I-beams. White noise is added to the calculated responses to simulate the polluted measurement as

$$v = v_{\text{calculated}}(1 + Ep\ Noise)$$

where v is the matrix of measured responses used in the identification; E_P is the noise level; *Noise* is a standard normal distribution vector with zero mean and unit standard deviation. $v_{\text{calculated}}$ is the set of calculated responses. The relative percentage error in the identified results are calculated by Eq. (22), where $\|\cdot\|$ is the norm of matrix, $P_{\text{identified}}$ and P_{true} are the identified and the true force time histories, respectively

$$\text{RPE} = \frac{\|P_{\text{identified}} - P_{\text{true}}\|}{\|P_{\text{true}}\|} 100\% \tag{22}$$

4.1 Validation of Proposed Method. A vehicle is modeled with a two-axle model with 4.26 m axle spacing. The axle loads are

Table 1 Natural frequency of the orthotropic bridge deck (in Hertz) The a denotes bending modes; *m* and *n* denote longitudinal and transverse mode number, respectively.

	n						
m	1	2	3	4	5	6	7
1	4.960[a]	6.310	10.015	16.074	24.814	33.650	45.264
2	19.842[a]	21.285	25.412	32.171	41.508	45.910	59.720
3	44.645[a]	46.067	50.325	57.329	67.059	68.449	81.124
4	79.369[a]	80.805	85.071	92.171	102.059	101.604	113.232
5	124.016[a]	124.024	125.424	125.443	125.463	145.215	146.056
	178.583[a]	179.316	181.572	185.484	191.117	191.165	191.454
7	243.074[a]	243.576	243.720	243.768	243.784	243.801	243.833

Table 2 Physical parameters of bridge deck

Concrete slab	I-beam	Diaphragm
Length $a=24.325$ m	beam spacing $b_1=2.743$ m	Diaphragms spacing $d=4.865$ m
Width $b=13.715$ m	web thickness $w_t=0.01111$ m	cross-sectional area $A=0.001548$ m^2
Height $h=0.2$ m	web height $w_h=1.490$ m	$I_y=0.707\times10^{-6}$ m^4
$E_x=4.1682\times10^{10}$ N/m^2	flange width $f_w=0.405$ m	$I_z=2\times10^{-6}$ m^4
$E_y=2.9733\times10^{10}$ N/m^2	flange thickness $f_t=0.018$ m	$J=1.2\times10^{-7}$ m^7
$\rho=3000$ kg/m^3	$\rho=7800$ kg/m^3	$\rho=7800$ kg/m^3
$\upsilon_{xy}=\upsilon_{yx}=0.3$		

$$P_1(t) = 6268[1.0 + 0.1\sin(10\pi t) + 0.05\sin(40\pi t)] \text{ kg}$$

$$P_2(t) = 12332[1.0 - 0.1\sin(10\pi t) + 0.05\sin(50\pi t)] \text{ kg}$$

The sampling frequency is 200 Hz, and the vehicle moves at 20 m/s along rail 3 at zero eccentricity. Nine modes are used in both the identification and the response analysis ($m=3$, $n=3$). Figure 3 shows the identified results using nine accelerations, nine velocities, and nine strains with 3% noise. The sensor patterns correspond to sensor arrangement SA9, 9-3, and 10, respectively, as shown in Fig. 4, with the sensors placed at the middle and quarter spans. Thirty-five sensor arrangements are listed in Fig. 4 and 28 of them will be used for study in Sec. 4.2. The relative percentage errors of the identified results for different noise level from nine accelerations in SA9, from a combination of six accelerations and three strains (SA8), and nine strains (SA10) are listed in Table 3. The following observations are made from Table 3 and Fig. 3:

- The relative percentage errors increase with the noise level. But the identified results from accelerations alone exhibit smaller errors than those from strains alone at the beginning and end of the time histories. This is because the acceleration responses capture the higher-frequency responses of the structure from the excitation of the force in the form of an impulsive force at entry of the bridge deck, whereas the strain responses retain only the lower-frequency responses, and thus causing larger error at the beginning of the identified force time histories.
- The first half of the identified time histories from nine accelerations match the true time histories very well, but they deviate from the true curves afterward. This is due to computation error in the solution process since the solution in a latter time step is dependent on that in the previous time step, and computation error would be accumulating over the complete time history leading to large error at the last time step.
- Error from the identification using accelerations comes from mainly the large fluctuation at the end of the time histories. Error from using velocities comes from mainly the fluctuations at both the start and end of the time histories, whereas error from using strains comes from these fluctuations as well as large fluctuations at higher frequencies throughout the duration of the time history. An inspection of the curves shows that a large proportion of them is contributed from the large fluctuations at both the start and end of the time history.
- The nine accelerations give better results than that from nine strains for a noise level up to 5%. There is a drastic increase in the error when the noise level increases up to 10%.
- The combination of six accelerations and three strains gives very good results for a noise level up to 5%.

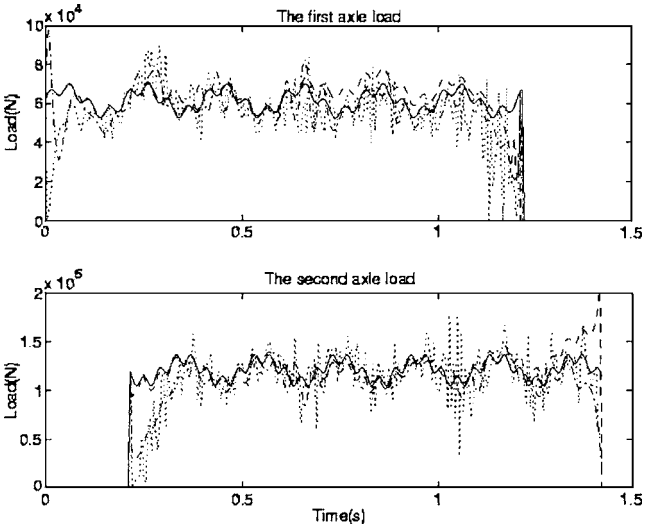

Fig. 3 Identification of axle loads with 3% noise (— true force, ---- nine accelerations, - · - · - nine velocities, …… nine strains)

4.2 Study on Effects of Sensor Type and Location. The above vehicle model is again used for this study. The loads move at a constant speed of 20 m/s along rails 3, 4, and 5 of the deck, in turn. To study the effect of different sensor arrangement and

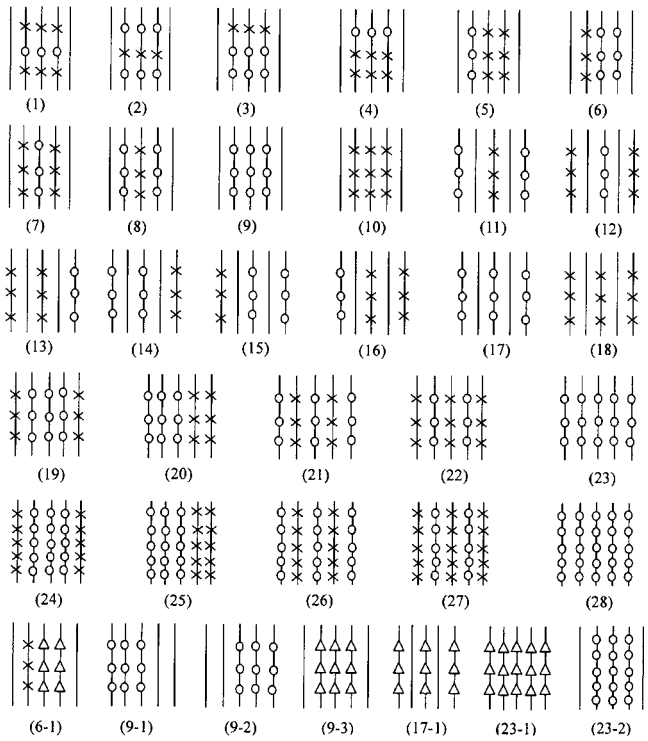

Fig. 4 Arrangements of strain gages and accelerometers for 9, 15, and 25 measured points (○ — accelerometer, △ — velocity sensor, × — strain gage)

Table 3 The relative percentage error (%) of identification with different noise level

Noise level (%)	From nine acceleratins (SA9)		From six accelerations and three strains (SA8)		From nine strains (SA10)	
	Axle 1	Axle 2	Axle 1	Axle 2	Axle 1	Axle 2
0	0.969	1.383	1.429	1.110	16.674	17.752
1	1.653	1.768	1.487	2.376	17.826	18.363
3	8.955	5.127	4.996	4.534	20.667	22.523
5	14.826	11.019	7.468	8.834	22.634	24.377
10	27.318	23.532	18.664	15.240	26.902	27.714

type of measured information on the identified results, 28 sensor arrangements (SA1 to 28) as illustrated in Fig. 4 are used in the simulation. Only the strain and acceleration measurements are studied. The five beams are drawn as solid dark lines in Fig. 4, and Rails 1–5 are named in sequence from left to right of the deck. There are three types of comparison on the effect of sensor arrangements:

(a) different type of sensors on the beam (SA1 to 4) versus same types of sensors on the beam (SA5 to 10)
(b) sensors on interior beams (SA5 to 10) versus sensors on edge beams (SA11 to 18)
(c) three sensors on all the beams (SA19 to 23) versus five sensors on all the beams (SA24 to 28)

The accelerometers and strain gages are placed at $a/4$, $a/2$, or $3/4a$ along the beams in SA1 to 23 and are evenly distributed along the beams in SA24 to 28. The number of modes for the identification and response analysis are nine ($m=3$, $n=3$) for nine sensors, fifteen ($m=3$, $n=5$) for fifteen sensors, and twenty-five ($m=5$, $n=5$) for twenty-five sensors. No noise is included in the analysis. The other conditions are the same as for Sec. 4.1. Table 4 shows the relative percentage errors of the identified results for the sensor arrangements and eccentricities of 0, $b/8$, and $3/8b$. The identified results from SA17 with *zero* and $3/8b$ eccentricities are plotted in Fig. 5.

The following observations are made from Table 4 and Fig. 5:

- The results identified from accelerations alone are better than those from strains alone, as well as many cases of combination of strain and acceleration. This observation is very prominent when the loads are moving at a large eccen-

Table 4 Relative percentage error (%) of identification from different sensor arrangements and eccentricities

Number of measured points	Sensor arrangement	*Eccentricity* (rail number)					
		0 (Rail 3)		$b/8$ (Rail 4)		$3/8b$ (Rail 5)	
		Axle 1	Axle 2	Axle 1	Axle 2	Axle 1	Axle 2
9	(1)	14.325	13.655	14.867	14.016	16.354	15.966
	(2)	6.354	5.985	6.890	6.372	9.087	8.653
	(3)	6.890	6.324	7.660	6.816	9.568	9.001
	(4)	13.695	13.243	14.358	13.654	15.001	14.760
	(5)	2.610	2.467	2.960	2.786	6.358	4.987
	(6)	1.102	1.206	1.246	1.405	2.726	2.502
	(7)	1.484	1.377	1.809	1.782	4.251	3.940
	(8)	1.429	1.110	1.954	1.552	2.814	2.324
	(9)	0.969	1.383	1.090	1.473	1.330	1.852
	(9–1)	0.934	1.314	2.045	2.385	18.631	19.055
	(9–2)	0.932	1.315	2.475	2.318	1.049	1.475
	(9–3)	15.372	16.410	15.916	17.058	16.754	18.890
	(10)	16.674	17.752	18.034	20.086	22.487	23.584
	(11)	0.662	0.781	2.883	2.870	10.815	11.203
	(12)	1.002	1.321	2.780	2.901	8.486	9.816
	(13)	1.966	2.110	3.784	3.975	4.886	5.219
	(14)	0.550	0.863	2.976	3.666	14.712	13.109
	(15)	0.542	0.796	1.421	1.285	3.724	3.330
	(16)	1.954	2.076	2.801	3.217	11.275	12.179
	(17)	0.480	0.565	0.741	1.252	2.510	2.902
	(17-1)	14.904	15.263	17.670	18.321	21.911	26.072
	(18)	16.180	16.783	17.867	19.036	29.214	30.505
15	(19)	1.320	0.938	1.572	1.206	1.965	1.516
	(20)	0.805	0.686	1.339	1.524	2.653	1.912
	(21)	0.742	0.625	1.089	1.207	2.917	2.098
	(22)	1.022	1.118	1.160	1.316	2.886	3.021
	(23)	0.543	0.825	1.680	1.116	2.904	2.464
	(23–1)	14.011	15.004	14.237	14.652	15.739	16.008
25	(24)	0.647	0.555	1.020	1.202	1.610	1.301
	(25)	0.673	0.587	1.188	1.541	1.580	1.579
	(26)	0.976	1.024	1.878	2.128	2.798	3.055
	(27)	0.760	0.649	2.867	3.022	1.682	1.740
	(28)	0.626	0.523	1.249	1.049	1.551	1.507

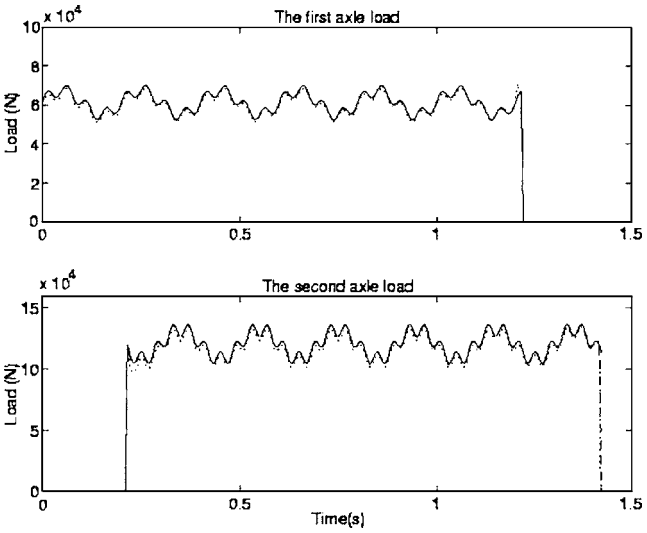

Fig. 5 Identification of axle loads from nine accelerations. (SA 17) (— true force, ---- with zero eccentricity, …… with 3/8*b* eccentricity)

tricity. This leads to the suspicion that the measured strain is not very sensitive to eccentric loads.

- Table 4 shows that when the same type of sensor is placed on the beam, the identified results would be more accurate compared to those having different sensors placed on the beam. This indicates that information of the same type should be obtained from all selected locations in the same beam for identification.
- Table 4 also shows that sensors on the edge beams do not give distinctly more accurate results compared to sensors on the interior beams.
- When the number of sensors is equal to the number of vibration modes for the identification, increasing the number of sensors does not significantly improve the identified result, in general, except for the case with large load eccentricity.
- This study demonstrates that optimal sensor type and location can be selected for an optimal identified result.

4.3 Further Studies on Sensor Location Effect and Velocity Measurement. Three more studies are conducted based on observations in Sec. 4.2.

(d) The last study is based on equal number of vibration modes in both the longitudinal and lateral directions and, thus, limiting the responses from only a single pattern of vibration modes for the identification. Sensor arrangement SA23 is studied again with comparison to a new arrangement SA23-2 as shown in Fig. 4. Both of them have 15 sensors while the former has five sensors in the lateral direction at $a/4$, $a/2$, or $3/4a$ along the beams, and the latter has five sensors evenly distributed on the beams in the longitudinal direction. Both arrangements have the sensors placed closed to the middle of the bridge deck. The effect from different combinations of vibration modes in the longitudinal and lateral directions of the bridge deck is studied. The same two-axle vehicle model and conditions for the previous studies are used, and the vehicle runs along rail 3. The relative percentage errors of identification for different load eccentricities are listed in Table 5.

Results from Table 5 show that

- The number of sensors in the lateral direction should be equal or greater than the number of lateral vibration modes used for the identification (case 2). The same conclusion is drawn for sensors in the longitudinal direction (case 5).
- When the load eccentricity is large, the torsional response of the structure is larger. A reduction in the number of lateral vibration modes for the identification from case 2 to case 1 would significantly affect the accuracy of results from SA23-2 but with little effect on SA23. Contrarily when the load eccentricity is small, the torsional response of the structure is smaller. A reduction in the number of longitudinal vibration mode from case 5 to case 4 does not have any significant effect on the results from the two sensor arrangements.

(e) Two other arrangements of sensors, SA9-1 and SA9-2, are further studied for the effect of unsymmetrically placed sensors on the identified results. All conditions are the same as for Sec. 4.2. The relative percentage errors of each identified axle load are shown in Table 4 and ($m=3$, $n=3$) mode combination is used. These results, as well as those from SA13 and 14, show that the identified results would be more accurate when the sensors are closer to the moving loads. They also confirm again that acceleration is more useful than strain measurements for the identification.

(f) Section 4.2 only studies the effectiveness of strain and acceleration measurements. The effectiveness of velocity measurement is therefore further studied here for comparison. SA9-3, 17-1, and 23-1 are studied, and they are compared with those from using strain and acceleration measurements. Errors in the identified loads in Table 4 clearly show that velocity is slightly better than strain measurements with comparable errors. Results from Sec. 4.1 also support this conclusion.

4.4 Effect of Aspect Ratio of Bridge Deck. To study the effect of the dimensions of the bridge deck on the identification, the width of the deck is kept constant at 13.715 m and the length

Table 5 Relative percentage error (%) of identification from different mode combinations and load eccentricities

Case	*m*	*n*	Total number of modes	*Eccentricity* (rail)					
				0 (Rail 3)		*b*/8 (Rail 4)		3/8*b* (Rail 5)	
				Axle 1	Axle 2	Axle 1	Axle 2	Axle 1	Axle 2
1	3	4	12	0.992/0.974	1.342/1.314	1.537/1.384	1.866/1.614	6.043/1.664	8.290/2.316
2	3	5	15	0.544/0.543	0.869/0.825	1.241/1.080	1.181/1.116	3.171/2.904	3.352/1.106
3	3	6	18	0.474/0.475	0.741/0.723	2.750/2.407	2.988/3.233	3.054/3.560	3.642/3.543
4	4	3	12	1.015/1.709	1.318/1.984	2.038/2.820	1.426/2.524	2.262/4.108	2.272/4.282
5	5	3	15	0.959/1.670	1.257/1.896	1.894/2.671	1.191/2.354	2.237/3.568	2.270/3.954
6	6	3	18	0.950/1.660	1.246/1.875	1.766/2.774	1.084/2.391	2.222/3.825	2.245/3.963

Note: •/• denotes results from sensor arrangement SA23-2 and SA23, respectively.

Table 6 Relative percentage error (%) of identification for different aspect ratio of the bridge deck

			Aspect ratio													
			0.5		1.0		1.5		2.0		2.5		5.0		10.0	
m	n	Total no. of modes	Axle 1	Axle 2	Axle 1	Axle 2	Axle 1	Axle 2	Axle 1	Axle 2	Axle 1	Axle 2	Axle 1	Axle 2	Axle 1	Axle 2
1	9	9	14.110	14.353	29.560	23.92	32.199	25.321	36.079	25.955	44.415	44.773	41.900	25.800	44.835	25.212
2	5	10	3.084	2.059	0.930	1.107	0.842	1.307	0.445	0.650	1.078	1.574	1.760	0.967	3.394	3.386
3	3	9	3.966	2.383	0.552	0.445	0.923	1.185	0.500	0.143	0.934	0.849	3.268	0.919	3.303	3.342
4	4	16	3.530	2.195	0.437	0.331	0.944	1.211	0.461	0.141	0.909	0.814	3.267	0.919	3.304	3.343

takes up different values of 6.868 m, 13.715 m, 20.573 m, 27.430 m, 34.288 m, 68.58 m, and 137.15 m, in turn, corresponding to an aspect ratio of 0.5, 1.0, 1.5, 2.0, 2.5, 5.0, and 10.0, respectively. The two-axle vehicle used for previous studies moves along rail 3. The number of modes used in identification is taken the same as for the response analysis but with different mode number in the longitudinal and lateral directions. Other conditions remain the same as for the last study. Table 6 shows the relative percentage errors of the identified results for SA9. The following observations are made:

- The use of only one longitudinal vibration modes for the identification does not give any meaning results for all the cases studied since three sensors in the lateral direction could not capture the nine lateral modes.
- Acceptable results can be obtained over a wide range of the aspect ratio from 1.0 to 5.0 as long as the number of longitudinal vibration modes is more than two.
- For the cases when the number of vibration modes is larger than the number of sensors, the accuracy of the identified result does not significantly improve.
- In practice, the vibration mode combination ($m=3$, $n=3$) could be obtained with accuracy, and this corresponds to the case with the least error in the study when the aspect ratio varies between 1.0 and 2.5, which is a practical range for ordinary bridge decks.

4.5 Further Study on Effect of Noise on Different Types of Measurements. Section 4.2 has included limited study on the noise effect on the load identification. Further study is made in this section to compare the effect of 10% noise on different types of response measurements from different patterns of sensor arrangement, i.e., SA 5, 6, 6-1, 9, 9-3, and 10 as listed in Fig. 4, and the relative percentage errors are listed in Table 7. This study makes use of the same two-axle vehicle for previous studies, and it moves along Rail 3. The ($m=3$, $n=3$) mode combination is used both in the identification and the response analysis, and other conditions remain the same for Sec. 4.2. The following observations are made:

- The errors in the identified forces are large for all the cases when only one type of measured information is used (SA9 and 10).
- When a mixture of measured information is used, acceleration performs better than velocity measurement.
- From the limited comparison in this study, the combination with more strain than acceleration measurements, i.e., six strains and three accelerations, give the smallest error in the identified forces.

Table 7 Relative percentage error (%) of identification with 10% noise for different types of measured information

	SA-5	SA-6	SA-6-1	SA-9	SA-9-3	SA-10
Axle 1	18.942	20.736	25.272	27.318	28.605	26.902
Axle 2	15.015	19.581	27.110	23.532	30.251	27.714

5 Experiment and Results

5.1 Experimental Setup. The model of a vehicle-bridge system fabricated in the laboratory is shown in Fig. 6. The bridge deck consists of a uniform steel plate (2.4384 m $\times$ 1.2192 m $\times$ 6.35 mm) stiffened with five rectangular ribs (25.4 mm $\times$ 12.5 mm) welded underneath the plate and simply supported at both ends on two steel I-beams, which, in turn, are fixed to the ground by bolts. Three U-shape aluminum sections were glued on the upper surface of the deck as a rail to guide the direction of the moving model vehicle. Rails 1, 2, and 3 correspond to $3/8b$, $b/8$, and zero eccentricities, respectively. The model vehicle was pulled along the rail by a string wound around the drive wheel of an electric motor. Nine photoelectric sensors are mounted evenly in a line on the deck at roughly equal intervals of 1 ft to check on the uniformity of the speed. Twenty strain gages are located at the bottom of the beams to measure the strain of the bridge deck as shown in Fig. 6 and six accelerators are located on the bottom at 1/4, 1/2, and 3/4 spans of beams 4 and 5. The model vehicle has four rubber wheels with fixed axle spacing of 0.457 m and wheel spacing 0.2 m. The front and rear axles weigh 5.2 kg and 14.7 kg, respectively. $p_1(t)$ and $p_3(t)$ are the left and right wheel loads at the front looking in the direction of the traveling path, $p_2(t)$ and $p_4(t)$ are the left and right wheel loads at the back following $p_1(t)$ and $p_3(t)$. A 16-channel data acquisition system and a KYOWA data record model RPT800A are used to collect the data in the experiments.

The rigidities of the equivalent orthotropic plate are $D_x = 7.3677 \times 10^4$ Nm, $D_y = 4.2696 \times 10^3$ Nm, and $D_k = 8.6018 \times 10^3$ Nm. The response is sampled at 1000 Hz, and the amount of data in each record segment is 7680. The average speed of the vehicle on the whole bridge deck is used for the identification of the moving loads in this study.

The p_{true} is not known in this practical case, and the relative percentage error (RPE) of the estimated forces is defined as

$$\text{RPE} = \frac{\|f_{j+1}^{\text{identify}} - f_j^{\text{identify}}\|}{\|f_j^{\text{identify}}\|} 100\% \tag{23}$$

where $f_j^{\text{identify}}, f_{j+1}^{\text{identify}}$ are the identified forces with λ_j and $\lambda_j + \Delta\lambda$. The value of λ that corresponds to the smallest relative percentage error is the optimal value [11–14].

5.2 Axle Load and Wheel Load Identification. The measured strains are resampled to have a time interval of 0.004 s. The model vehicle is moving at 1.11 m/s along rails 1, 2, and 3, in turn. The sensor sets adopted in the identification are shown in Table 8, and the number of modes employed in the identification

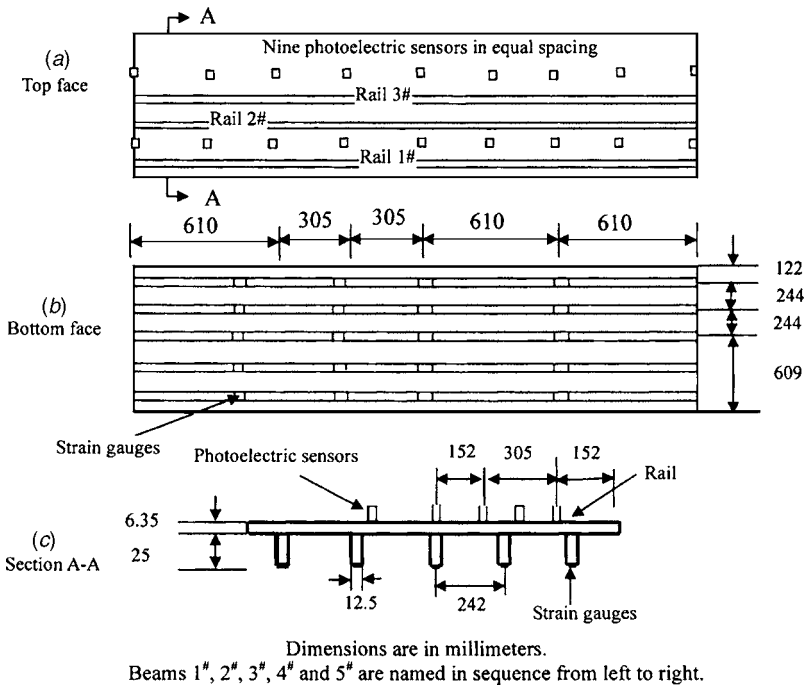

Dimensions are in millimeters.
Beams 1#, 2#, 3#, 4# and 5# are named in sequence from left to right.

Fig. 6 Layout of the bridge deck in experiment

is equal to the number of sensors, i.e., nine modes ($m=3$, $n=3$) for nine sensors, 12 modes ($m=3$, $n=4$) for 12 sensors, 15 modes ($m=5$, $n=3$) for 15 sensors, and 20 modes ($m=4$, $n=5$) for 20 sensors.

Figures 7 and 8 show the identified wheel loads, axle loads, and the total vehicle load compared to the corresponding static loads when the model vehicle moves along rail 3 from sensor set 7. The correlation coefficients between the measured and the reconstructed strain responses at $3/8a$ of each beam are tabulated in Table 9.

Table 9 and Figs. 7 and 8 exhibit the following observations:

- The combination of strains and accelerations give better results than the same number of strains alone, and the accuracy of identified axle loads is higher than that for the wheel loads.
- When the number of sensors is equal to the number of vibration modes in the identification, the use of more sensors does not improve the accuracy of the results significantly.
- When the vehicle moves along rail 1, the correlation coefficients between the measured and the reconstructed strain responses at $3/8a$ of beam 1 is very poor, the others are all above 0.88. This is due to the low signal-to-noise ratio in the sensors further away from the moving loads giving less accurate results.

6 Discussions

6.1 Comparison to Existing Methods. The authors have also solved the moving load identification problem using the dynamic programing method [16] making use of velocity and strain measurements. But in the proposed approach, acceleration, velocity, and strain measurements can be used as input, which is more flexible for practical use. This study compares the effectiveness and accuracy of load identification using this method to the dynamic programing method. The measured strains are resampled to have a time interval of 0.005 s. The model vehicle is moving at 1.11 m/s along rail 3. Fifteen vibration modes are employed in

Table 8 Sensor sets for moving load identification in experiment

Sensor set	Total number ofsensors	Sensor type and number	Sensor location	
			Transverse	Longitudinal
1	9	6 strains	Beams 2 and 3	$\frac{1}{4}$, $\frac{1}{2}$, $\frac{3}{4}$ spans
		3 accelerations	Beam 4	-ditto-
2	9	9 strains	Beams 2, 3, and 4	$\frac{1}{4}$, $\frac{1}{2}$, $\frac{3}{4}$ spans
3	9	6 strains	Beams 1 and 3	$\frac{1}{4}$, $\frac{1}{2}$, $\frac{3}{4}$ spans
		3 accelerations	Beam 5	-ditto-
4	9	9 strains	Beams 1, 3, and 5	$\frac{1}{4}$, $\frac{1}{2}$, $\frac{3}{4}$ spans
5	12	6 strains	Beams 1 and 2	$\frac{1}{4}$, $\frac{1}{2}$, $\frac{3}{4}$ spans
		6 accelerations	Beams 4 and 5	-ditto-
6	12	12 strains	Beams 1, 2, 4, and 5	$\frac{1}{4}$, $\frac{1}{2}$, $\frac{3}{4}$ spans
7	15	9 strains	Beams 1, 2, and 3	$\frac{1}{4}$, $\frac{1}{2}$, $\frac{3}{4}$ spans
		6 accelerations	Beams 4 and 5	-ditto-
8	15	15 strains	Beams 1, 2, 3, 4, and 5	$\frac{1}{4}$, $\frac{1}{2}$, $\frac{3}{4}$ spans
9	20	20 strains	Beams 1, 2, 3, 4, and 5	$\frac{1}{4}$, $\frac{3}{8}$, $\frac{1}{2}$, $\frac{3}{4}$ spans

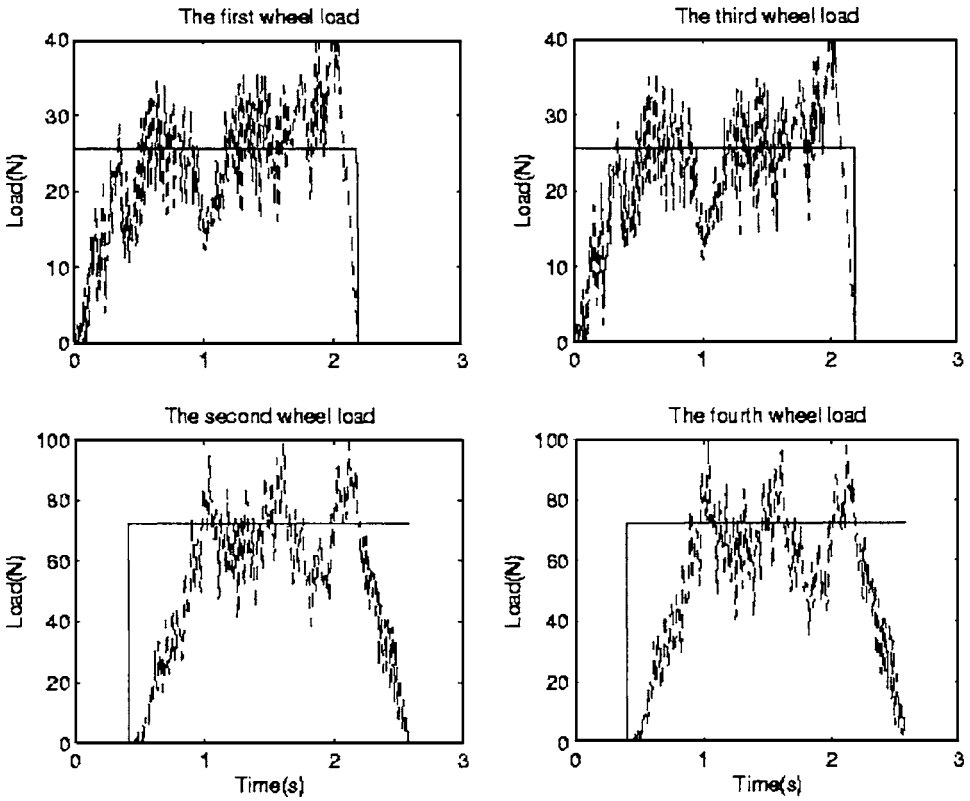

Fig. 7 Identification of wheel loads from the measured responses (sensor set 7) (— static load, ---- identified load)

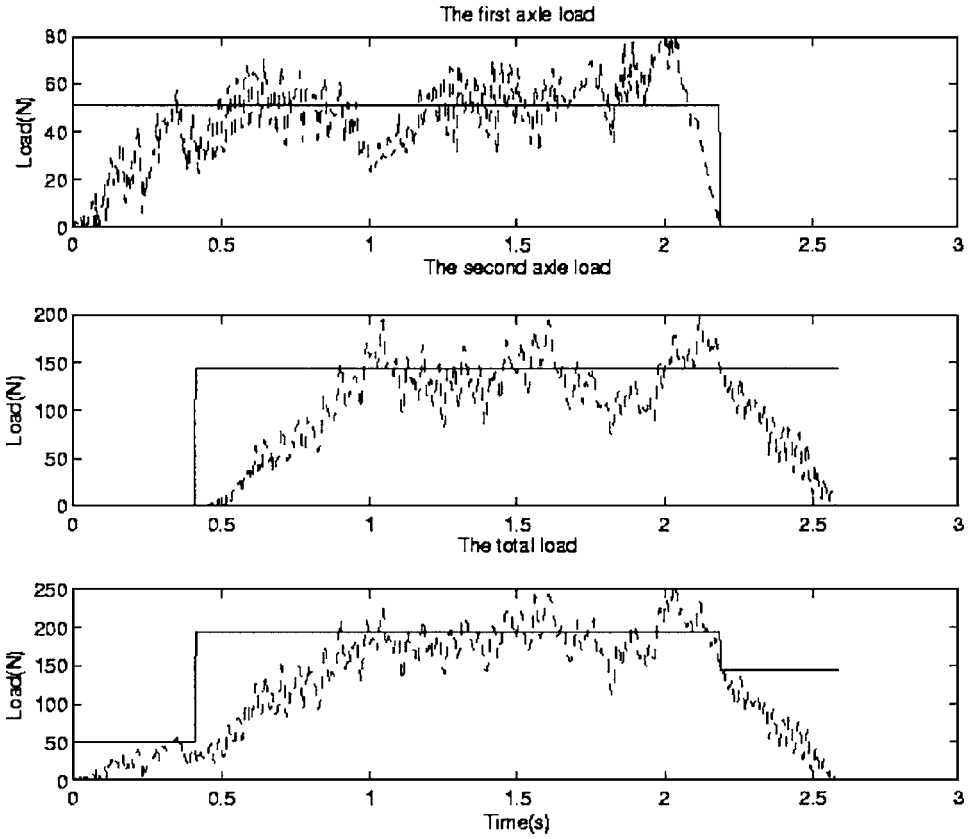

Fig. 8 Identification of axle and total loads from the measured responses (sensor set 7) (— static load, ---- identified load)

Table 9 Correlation coefficients of measured and reconstructed strains from different sensor sets and load eccentricities

Eccentricity (Rail no.)	Sensor sets	Beam 1	Beam 2	Beam 3	Beam 4	Beam 5
0	1	–	0.978	0.968	0.979	–
(Rail 3)	2	–	0.922	0.921	0.923	–
	3	0.970	–	0.971	–	0.964
	4	0.925	–	0.927	–	0.925
	5	0.970	0.981	–	0.981	0.965
	6	0.931	0.933	–	0.933	0.930
	7	0.971	0.983	0.985	0.983	0.970
	8	0.930	0.931	0.933	0.931	0.931
	9	0.932	0.932	0.935	0.932	0.930
1/8 *b*	1	–	0.932	0.930	0.931	–
(Rail 2)	2	–	0.900	0.919	0.910	–
	3	0.902	–	0.923	–	0.930
	4	0.886	–	0.919	–	0.916
	5	0.911	0.926	–	0.931	0.933
	6	0.889	0.910	–	0.918	0.919
	7	0.904	0.928	0.932	0.935	0.930
	8	0.885	0.907	0.916	0.920	0.918
	9	0.884	0.906	0.908	0.916	0.912
3/8 *b*	1	–	0.903	0.909	0.944	–
(Rail 1)	2	–	0.880	0.890	0.911	–
	3	0.300	–	0.909	–	0.944
	4	0.199	–	0.897	–	0.925
	5	0.311	0.908	–	0.954	0.956
	6	0.205	0.886	–	0.913	0.927
	7	0.303	0.902	0.922	0.961	0.967
	8	0.208	0.887	0.896	0.916	0.929
	9	0.211	0.890	0.899	0.919	0.931

Note: – denotes case not studied.

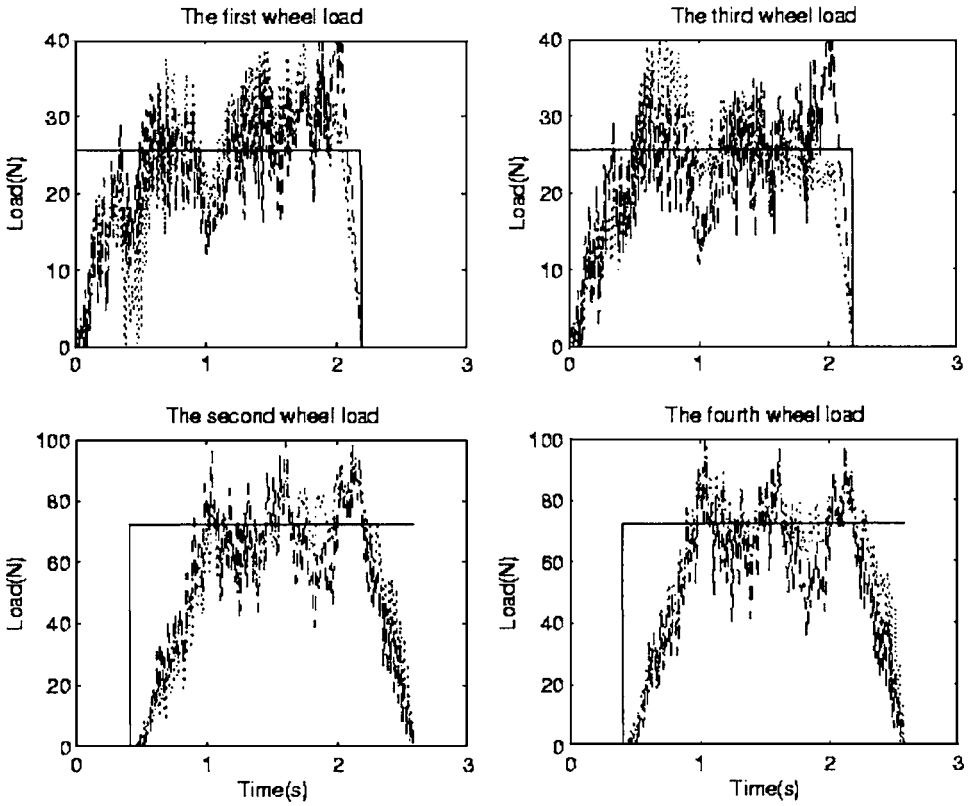

Fig. 9 Identification of experimental wheel loads from the measured responses (sensor set 8) (— static load, ---- proposed method, …… dynamic programing method)

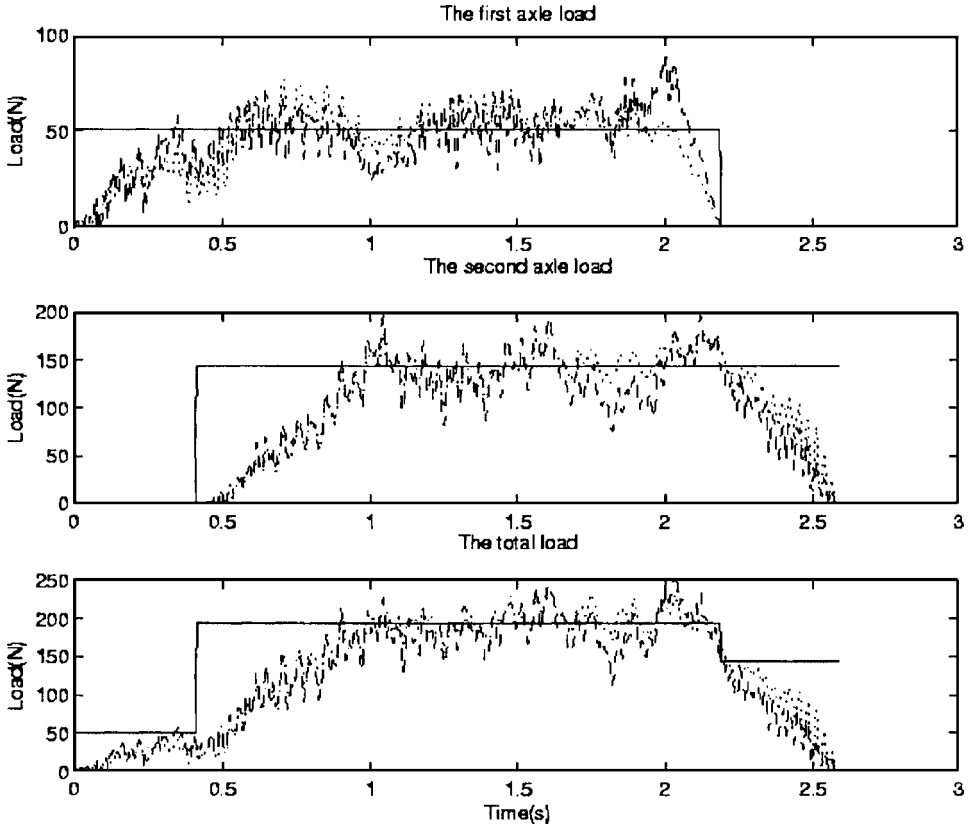

Fig. 10 Identification of experimental axle and total loads from the measured responses (sensor set 8) (— static load, ---- proposed method, …… dynamic programing method)

the identification ($m=3$, $n=5$). The identified results calculated by the proposed method from Eq. (23) and by the dynamic programing method from sensor set 8 listed in Table 8 are plotted in Figs. 9 and 10. The identified results from the two methods are almost the same throughout the time histories. The proposed method takes 185 s to complete, whereas the dynamic programing method takes 235 s to complete using MATLAB with a 2.4 GHz Pentium-4 PC and 512 M RAM.

Another comparison has been made to another moving load identification method developed by the authors [8], which is also based on an analytical approach in the solution as the present one. The bridge deck shown in Fig. 2 is used in the comparison. The length of the bridge deck is 24.325 m. Other parameters are the same as those in the previous numerical study in Sec. 4. Acceleration obtained from the sensor arrangement SA9 in Fig. 4 is used in the simulation, and the moving loads are moving along rail 2. The time interval between adjacent data point is 0.005 s. Table 10 shows the error of identification in the moving loads using the present method and that by Zhu and Law [8]. Nine ($m=3$, $n=3$) and fifteen ($m=3$, $n=5$) vibration modes are used in the comparison study, and three types of noise levels are included. Results show that the present method gives much better results than Zhu and Law [8] with less computation time varying from 15% to 100%.

6.2 Discussion on the Effect of Modeling Error. It is always difficult to have an exact finite element model of the structure in practice, and the modeling error would affect the identification results in terms of errors in the modal frequencies and the mode shape functions in Eq. (5). A previous study with an exact solution to the problem [11] using a polluted set of mode shapes and modal frequencies in the identification show that when only the first six modes are available, a reasonably accurate set of identified moving loads can still be obtained.

7 Conclusions

A new moving load identification method formulated in state space with regularization on the solution is presented. It is more suitable for practical application than existing methods because of the flexibility in the type of dynamic response input. The bridge

Table 10 Percentage errors in the identified results by the present method and that by Zhu and Law [8]

	Zhu and Law [8]						Present method					
	$m=3$, $n=3$			$m=3$, $n=5$			$m=3$, $n=3$			$m=3$, $n=5$		
Vibration modes	Axle 1	Axle 2	Time (s)	Axle 1	Axle 2	Time (s)	Axle 1	Axle 2	Time (s)	Axle 1	Axle 2	Time (s)
1 % noise	10.59	5.48	148	6.39	3.53	290	2.11	1.82	122	1.62	1.41	179
3 % noise	24.37	14.00	155	12.79	7.96	301	5.92	4.99	99	2.84	2.15	172
5 % noise	38.48	22.54	152	17.92	10.65	234	10.38	8.42	76	4.17	3.16	176

deck is modeled as an orthotropic rectangular plate, and the loads are modeled as a group of loads moving on top of the bridge deck at a fixed distance and at a constant speed. The Hamilton principle and the modal superposition principle are included in the formulation. Numerical simulations and experimental tests are employed for the verification and illustration on the effectiveness of the proposed method. The effects of sensor location, different load path eccentricity, different types of measured information, measurement noise, and the aspect ratio of the bridge deck have been studied. The following conclusions are made.

- The proposed approach is effective to identify either axle loads or individual wheel loads moving on top of the bridge deck from measured responses, and acceptable results can be obtained.
- For the present study, the acceleration response and the combination of the acceleration and strain responses would give better results than an equal number of strain or velocity measurements, particularly for loads moving at a large eccentricity.
- When a mixture of measured information is used for the identification, information of the same type should be obtained from all sensor locations in the same beam to have more accurate results.
- Sensors placed closer to the moving load would give more accurate results than sensors further away from the moving loads.
- Nine vibration modes ($m=3$, $n=3$) can usually be measured accurately from most of the bridge decks, and when nine sensors are used, the proposed identification method gives good results over the practical range of aspect ratio of the bridge deck.

Acknowledgment

The work described in this paper was supported by a grant from the Hong Kong Research Grant Council Project No. PolyU 5043/02E and a grant from the Hong Kong Polytechnic University Project No. G-YW98.

References

[1] Moses, F., 1984, "Weigh-in-Motion System Using Instrumented Bridge," J. Transp. Eng., **105**, pp. 233–249.
[2] Law, S. S., Chan, T. H. T., and Zeng, Q. H., 1997, "Moving Force Identification: Time Domain Method," J. Sound Vib., **201**(1), pp. 1–22.
[3] Law, S. S., Chan, T. H. T., and Zeng, Q. H., 1999, "Moving Force Identification: A Frequency and Time Domains Approach," ASME J. Dyn. Syst., Meas., Control, **121**(3), pp. 394–401.
[4] Zhu, X. Q., and Law, S. S., 1999, "Moving Force Identification on a Multi-Span Continuous Bridge," J. Sound Vib., **228**(2), pp. 377–396.
[5] Yuan, X. R., Chen, E. L., and Yang, S. P., 1998, "Moving Loads Identification Through Responses of Orthotropic Plate," J. Vib. Meas. Diagnosis, **18**(3), pp. 201–205.
[6] Jiang, R. J., Au, F. T. K., and Cheung, Y. K., 2004, "Identification of Vehicles Moving on Continuous Bridges With Rough Surface," J. Sound Vib., **274**(3–5), pp. 1045–1063.
[7] Zhu, X. Q., and Law, S. S., 2003, "Time Domain Identification of Moving Loads on Bridge Deck," ASME J. Vibr. Acoust., **125**(2), pp. 187–198.
[8] Zhu, X. Q., and Law, S. S., 2001, "Identification of Moving Loads on an Orthotropic Plate," ASME J. Vibr. Acoust., **123**(2), pp. 238–244.
[9] Juang, J.-N., 1994, *Applied System Identification*, Prentice Hall, Englewood Cliffs, NJ.
[10] Pesterev, A. V., Bergman, L. A., Tan, C. A., and Yang, B., 2004, "Assessing Tire Forces due to Roadway Unevenness by the Pothole Dynamic Amplification Factor Method," J. Sound Vib., in press.
[11] Zhu, X. Q., and Law, S. S., 2002, "Moving Loads Identification Through Regularization," J. Eng. Mech., **128**(9), pp. 989–1000.
[12] Busby, H. R., and Trujillo, D. M., 1997, "Optimal Regularization of an Inverse Dynamics Problem," Comput. Struct., **63**(2), pp. 243–248.
[13] Trujillo, D. M., and Busby, H. R., 1997, *Practical Inverse Analysis in Engineering*, CRC Press, Boca Roton.
[14] Carlos Santamarina, J., and Fratta, D., 1998, *Introduction to Discrete Signals and Inverse Problems in Civil Engineering*, ASCE, Reston, VA.
[15] Tikhonov, A. N., and Arsenin, V. Y., 1977, *Ill-Posed Problems*, Wiley, New York.
[16] Law, S. S., Bu, J. Q., Zhu, X.Q., and Chan, S. L., "Moving Loads Identification From Velocity and Strain Measurements," J. Sound Vib., under review.